Modeling postcritical two-phase heat transfer in EcosimPro/ESPSS environment

GLASGOW, SCOTLAND | 20-23 MAY 2024

Matteo Fiore[(1)], **Marco Fabiani**[(1)], **Francesco Nasuti**[(1)]

[(1)] Sapienza University of Rome, Rome, Italy
Email: matteo.fiore@uniroma1.it, m.fabiani@uniroma1.it, francesco.nasuti@uniroma1.it

KEYWORDS: Flow boiling, regenerative cooling, liquid rocket engines

ABSTRACT:
Flow boiling in cooling channels is a complex phenomenon due to the wide range of flow patterns that can emerge during coolant vaporization, resulting in various heat transfer regimes. To provide reliable yet efficient simulations for accurate estimation of coolant heat transfer capabilities in support of liquid rocket engine design, a new model for two-phase heat transfer has been implemented in the EcosimPro/European Space Propulsion System Simulation (ESPSS) tool. The accuracy of this model has been validated against experimental data for cryogenic fluids, focusing on wall temperature prediction and Critical Heat Flux (CHF) position. A comparison with the built-in model available in the EcosimPro software was also conducted. Results indicate that the built-in model can lead to significant inaccuracies in wall temperature predictions due to the lack of proper CHF modeling. Conversely, the new model shows substantial improvement in predictive capabilities, especially in cases where CHF occurs at the channel inlet.

1. Introduction

Given the challenges posed by a new era of space exploration, the space propulsion community needs to enhance engine design and analysis techniques, particularly when exploring new concepts or propellants. It is particularly important to highlight the role of reduced-order modeling techniques, particularly during the initial design stages. In this setting, the presence of the ESPSS toolkit is rather advantageous. It is a standardized European resource that facilitates the design, analysis, and simulation of space propulsion systems. It is based on the EcosimPro framework and has been developed by ESA since 2006 [1]. Thanks to the versatility of the EcosimPro platform the component libraries can be improved by the users for specific goals. This is the case of the problem of two-phase heat transfer which is faced in the present study. Indeed, even if fluids exploited in cooling systems for liquid rocket engines, typically operate under supercritical design pressure conditions, in essential phases like those of planetary landing or in reusable rocket systems during transient phases such as chill-down, engine start-up and shut-down, or controlled engine operations, two-phase flow conditions including flow boiling are likely to occur. Predicting the heat transfer coefficient under these conditions presents significant challenges, because changes to any of the system parameters - including mass flux, inlet quality, pressure, heat flux, tube diameter, or orientation - can significantly affect flow evolution and heat transfer capabilities. The ESPSS toolkit currently incorporates models for simulating two-phase flows, yet lacks appropriate models for film boiling in annular regimes commonly encountered in cryogenic flow boiling. However, existing models are limited in either selecting proper correlations for flow boiling or implementing suitable transitions between heat transfer regimes. The consequence is that they yield significant errors in wall temperature predictions. For this reason, adopting a comparable approach as suggested in [2], the present work focuses on the implementation of two-phase heat transfer correlations in EcosimPro/ESPSS environment, able to improve the current heat transfer coefficient function in post-Critical Heat Flux (CHF) regimes. A criterion to switch between the different heat transfer regimes has been implemented, identifying the CHF location through suitable correlations developed for cryogenic fluids. Correlations available in the literature, derived from forced convection boiling data and with cryogenic fluids, are tested in the film boiling regime, while the correlation of Chen has been kept for the nucleate boiling regime. Experimental tests on heated pipes with hydrogen and nitrogen as working fluids have been replicated [3–5], to test the new component, as well as to perform an assessment of correlations selected for CHF identification and post-CHF heat transfer.

2. Flow boiling

Assuming a tube uniformly heated over its length, fed with subcooled liquid at a mass flow such that the fluid completely vaporizes, there can be different flow evolution patterns within the pipe depending on the flow rate, enforced heat flux, pipe geometry and orientation. Multiple flow patterns can appear and evolve as a consequence of the vapour quality variation in the pipe, each of which has a specific impact on pressure drop and heat transfer [6].

Following the map of heat transfer regimes reported in Fig. 1 (curve I) when the wall temperature reaches the value that allows the formation of the first vapour bubble in the nucleation site, the nucleate boiling heat transfer mechanism begins. This condition is defined as Onset of Nucleate Boiling

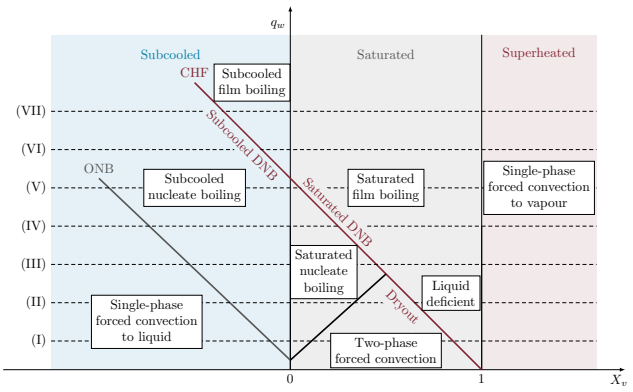

Figure 1: Flow boiling heat transfer map.

(ONB). As the bulk vapour fraction increases, the collision and coalescence between bubbles results in larger bubbles that eventually fill the tube diameter until at some point the transition between nucleate boiling and two-phase force convection takes place. In this case there is the suppression of boiling at wall and heat is removed by forced convection of the liquid film and then transferred to the vapour core by evaporation of the liquid-vapour interface. At some point the complete evaporation of the liquid film occurs and the dryout condition takes place, which is a form of CHF. This condition yields a sharp rise of wall temperature as no more liquid is in contact with the wall, leading to a sudden decrease of heat transfer capabilities. After this point there is the so called liquid deficient region where there are only fine dispersed liquid droplets and this region extents until the liquid is fully vaporized. Here, the process of heat transfer is the single phase forced convection to the vapour phase.

The above comments hold to the case when a relative low heat flux is supplied to the wall. When increasing heat flux, the ONB occurs sooner, as well as dryout (curve II). However, as the quality increases, before the two-phase convection region initiates and while bubble nucleation is still occurring, another mechanism of CHF takes place, which is similar to the boiling crisis in pool boiling and is termed Departure from Nucleate Boiling (DNB), curves (III-VII). At DNB the critical conditions are reached at the wall because of localized coalescence of vapour bubbles into a vapour film, even at axial locations with subcooled liquid flow in the core, curves (VI,VII). The larger the heat flux the earlier the DNB will occur. The vapour precludes liquid access from the core to the wall and, because of high wall heat flux, causes the wall temperature to rapidly rise. Downstream the DNB, film boiling region is present until 100% of vapour is formed. For DNB-type CHF, the pre-CHF region is characterized just by a bubbly flow with small vapour bubbles present in neighborhood of the wall, while, downstream the CHF point, an inverted annular flow is observed first, which is comprised of a liquid core surrounded by a vapour film covering the pipe wall, then the liquid core breaks up and only fine dispersed liquid droplets survive until a complete vaporization is reached. A schematic of flow patterns and heat transfer regimes during flow boiling can be observed in Fig. 2.

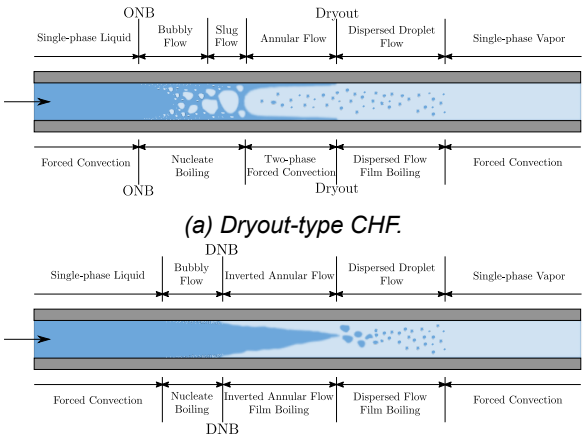

(a) Dryout-type CHF.

(b) DNB-type CHF.

Figure 2: Schematic of CHF mechanisms during flow boiling.

3. Built-in model

The ESPSS libraries present in EcosimPro provide the capability of simulating cryogenic two phase flows, employing the Homogeneous Equilibrium Model (HEM). The two-phase flow is modeled as a mixture of vapour and liquid, which are assumed to have the same temperature, pressure and velocity. As a result, the same equations (mass, momentum and energy conservation) that are used for a single-phase flow are employed. The vapour mass fraction (quality) is computed from thermodynamic considerations as reported in Eq. 1.

$$X_v = \frac{h - h_f}{h_g - h_f} \tag{1}$$

where h is the enthalpy of the mixture, and h_f and h_g are respectively the enthalpy of saturated liquid and vapour at the mixture pressure.

The heat transfer from the flow to the wall is computed according to Eq. 2.

$$q = h_c \left(T_w - T_b\right) \tag{2}$$

where q is the heat flux, h_c is the heat transfer coefficient, T_b the fluid bulk temperature and T_w the wall temperature. Tube components offer multiple options to compute h_c. Specifically two formulations can deal with two-phase flows: namely `ht_tube` and `ht_boiling`. However, since the `ht_boiling` function is based on pool boiling correlations, it is unable to model forced convection regimes. Therefore, it has not been evaluated in this study. Consequently, the results labeled as *Built-in* have been generated using the `ht_tube` option.

3.1. *ht_tube* option

A schematic representation of the `ht_tube` option is reported in Fig. 3 for both flow boiling and condensation.

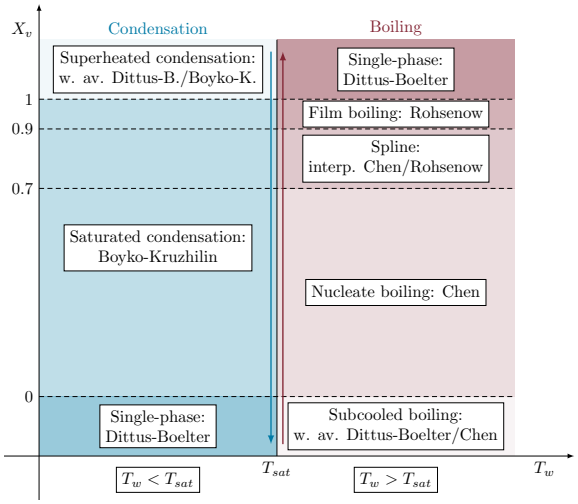

Figure 3: ht_tube heat transfer model.

Specifically, for flow boiling conditions, the specific regime and the corresponding correlation for the evaluation of the heat transfer coefficient is selected according to the value of the bulk vapor mass fraction. It can be noted that the nucleate boiling regime is selected as long as $X_v < 0.7$ and the heat transfer coefficient is calculated through the correlation of Chen [7]. Conversely, when $X_v > 0.9$, the film boiling regime is chosen and the heat transfer coefficient is calculated based on the correlation developed by Dougall-Rohsenow [8]. For $0.7 < X_v < 0.9$, the transition boiling regime is selected, and the heat transfer coefficient is determined through spline interpolation between the nucleate boiling and film boiling coefficients. It is worth to point out that in the `ht_tube` option, no appropriate model is available for the CHF prediction. As a matter of fact, the use of the vapour mass fraction as a discriminant to switch between models may lead to significant errors, since X_v is not a parameter which clearly identifies a heat transfer regime. This can yield significant errors in the prediction of the wall temperature.

4. New Model

From an analysis of the correlations available in the ESPSS libraries and of the literature, appropriate correlations are needed. Such correlations need to be derived/fitted from forced convection boiling data (and not pool boiling) and possibly with cryogenic fluids, in order to correctly simulate flow boiling with a reduced order numerical model. To avoid possible numerical issues arising from the sudden change of heat transfer coefficients in a transient simulation, a steady component will be derived as a modification of the conventional steady 1D pipe [1].

A first step is to implement a more realistic criterion to switch between the different heat transfer regimes rather than employing the bulk vapour faction. For this purpose, the location of the CHF can be either manually provided by the user or calculated by suitable correlations. Two correlations have been selected and tested for the calculation of the CHF position. They are reported in Tab. 1 and results will be discussed in Section 7.3.

The universal correlation of *Ganesan* [9] has been developed after the compilation of a database made from experimental data about CHF in uniformly heated pipes with cryogenic fluids like hydrogen, nitrogen, helium and methane. For the given enforced heat flux, the channel axial location where CHF occurs x_{CHF} is directly calculated according to relations reported in Tab. 1. On the other hand, the correlation of *Shah* [10] does not directly provide the location of CHF for a given heat flux, but rather the critical heat flux for a given axial location. Hence the CHF position is selected as the position where the calculated critical heat flux becomes lower than the enforced heat flux. Once the location where the boiling crisis occurs, if any, there is a switch between the nucleate boiling regime and the film boiling regime.

For the new heat transfer model, the correlation of Chen has been kept for the nucleate boiling regime while different correlations have been tested and compared for the film boiling regime, which are essentially suitable modifications of the Dittus-Boelter correlation for turbulent single-phase forced convection. These correlations are reported in Tab. 2.

In addition to well-known film boiling correlations, recently developed universal correlations specifically tailored for cryogenic fluids [11], have also been tested. However, it is crucial to note that the correlations selected for the post-CHF regime may have limitations, particularly when CHF occurs at small values of X_v. In such conditions, the heat transfer coefficient tends to zero and thus the resulting wall temperature could approach infinity. Additionally, these correlations are not applicable in cases of subcooled film boiling conditions (i.e. $X_v \leq 0$). As a result, due to the absence of suitable correlations for subcooled film boiling conditions, a lower limit of $X_{v,min} = 0.01$ has been arbitrarily set for the vapour fraction used in evaluating the heat transfer coefficient within the film boiling regime. Eventually, to provide a smooth transitions between heat transfer regimes, smoothing functions have been employed.

5. Reference data

To test the new component, as well as to perform an assessment of the film boiling correlations selected, experimental tests on post-CHF flow boiling in uniformly heated pipes have been selected from the open literature. Special attention has been devoted to experimental data concerning cryogenic propellants, which are fluids of interest in the present re-

Table 1: CHF correlations.

Ganesan [9]	$x_{CHF} = D\left(\frac{c_1 \mathrm{We}_{fo,D}^{c_2}\left(\frac{\rho_f}{\rho_g}\right)^{c_3}(1-X_{v,in})^{1+c_4}}{4\mathrm{Bo}}\right)^{\frac{1}{1-c_5}}$ $\mathrm{We}_{fo,D} = G^2 D/(\rho_f \sigma)$, $\mathrm{Bo} = q/(Gh_{fg})$ DNB-type CHF: $c_1 = 0.17,\ c_2 = -0.21,\ c_3 = -0.32,\ c_4 = 1.07,\ c_5 = 0.59$ Dryout-type CHF: $c_1 = 0.9,\ c_2 = -0.22,\ c_3 = -0.19,\ c_4 = 1.68,\ c_5 = 0.21$
Shah [10]	$q_{CHF,U} = 0.124 Gh_{fg}\left(\frac{D}{L_E}\right)^{0.89}\left(\frac{10^4}{Y}\right)^n(1-X_{v,in,E})$ $q_{CHF,L} = Gh_{fg}F_E F_x \mathrm{Bo}_{X_{v,CHF}=0}$ $Y = \left(\frac{GDc_{p,f}}{k_f}\right)\left(\frac{G^2}{\rho_f^2 gD}\right)^{0.4}\left(\frac{\mu_f}{\mu_g}\right)^{0.6}$ If $Y \leq 10^6$ then $q_{CHF} = q_{CHF,U}$ else if $Y > 10^6$ and $L_E > 160/p_r^{1.14}$ then $q_{CHF} = q_{CHF,U}$ else if $Y > 10^6$ and $L_E \leq 160/p_r^{1.14}$ then $q_{CHF} = \min(q_{CHF,L}\ ,\ q_{CHF,U})$ If $X_{v,in} \leq 0$ then $L_E = x_{CHF}$, $X_{v,in,E} = X_{v,in}$ else $L_E = x_{CHF} + \frac{X_{v,in}D}{4\mathrm{Bo}}$, $X_{v,in,E} = 0$ If $Y < 10^4$ then $n = 0$ else if $10^4 < Y < 10^6$ then $n = \left(\frac{D}{L_E}\right)^{0.54}$ else $n = \frac{0.12}{\sqrt{1-X_{v,in,E}}}$ $F_E = \max(1\ ,\ 1.54 - 0.032\frac{x_{CHF}}{D})$ If $X_{v,CHF} > 0$ then $F_x = F_3\left[1 + \frac{(F_3^{-0.29}-1)(p_r-0.6)}{0.35}\right]^c$ else $F_x = F_1\left[1 - \frac{(1-F_2)(p_r-0.6)}{0.35}\right]^c$ $F_3 = \left(\frac{1.5\cdot 10^5}{Y}\right)^{0.833 X_{v,CHF}}$ $\quad F_1 = 1 + 0.0052\left(-X_{v,CHF}^{0.88}\right)\left[\min(1.4\cdot 10^7\ ,\ Y)\right]^{0.41}$ If $p_r \leq 0.6$ then $c = 0$ else $c = 1$ $\quad$ If $F_1 \leq 4$ then $F_2 = F_1^{-0.42}$ else $F_2 = 0.55$ $\mathrm{Bo}_{X_{v,CHF}=0} = \max(15Y^{-0.612}\ ,\ 0.082Y^{-0.3}(1+1.45p_r^{4.03})\ ,\ 0.0024Y^{-0.105}(1+1.15p_r^{3.39}))$

search activity. Although the literature is quite poor given the difficulties needed to deal with this category of fluids, the experimental works of *Hendricks et al* [3], *Lewis et al* [4] and *Forslund et al* [5]. have been deemed suitable for the present study. In their work, they performed studies on film boiling involving hydrogen and nitrogen in a vertical upflow configuration. The experimental setups are quite similar, consisting of a pipe uniformly heated by an electrical power supply. The pipes are characterized by a diameter of 7.95 mm, 14.1 mm and 8.2 mm and a length of about 0.3 m, 0.4 m and 1.2 m, respectively, for [3], [4] and [5]. Different types of sensors are mounted on the test section providing measurements of mass flow rate, static pressure, fluid temperature, and wall temperature distribution. Multiple runs have been chosen from the experimental works. Specifically 15 test cases have been simulated from [3], 28 from [4] and 12 from [5]. A summary of the operative conditions for each test case is reported in Tab. A1.

6. EcosimPro Schematic

The schematic which has been used for the present analysis is reported in Fig. 4 and is characterized by the new component, where the user can set the correlations for each heat transfer regime, a heater that enforces the the desired power to the tube walls, inlet and outlet components to enforce the desired boundary conditions in terms of pressure and temperature and a junction component which essentially represents an orifice with imposed mass flow.

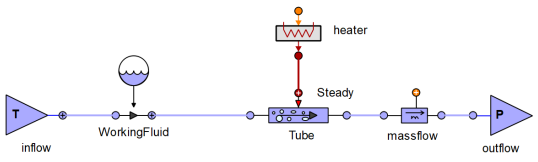

Figure 4: EcosimPro schematic adopted for the simulations.

Table 2: Film boiling correlations.

Ganesan (eq) [11]	$h_{\text{tp}} = c_1 h_{DB,g} (\text{Bo}^*)^{c_2}$ $h_{DB_g} = 0.023 \frac{k_g}{D} \text{Re}_g^{0.8} \text{Pr}_g^{0.4}, \quad \text{Re}_g = \frac{GDX_v}{\mu_g}, \quad \text{Pr}_g = \frac{\mu_g c_{p,g}}{k_g}, \quad \text{Bo}^* = \frac{X_v - X_{v,in}}{1 - X_{v,in}}$ $\underbrace{c_1 = 0.7484,\ c_2 = -0.4133}_{IAFB} \quad \underbrace{c_1 = 0.5236,\ c_2 = -0.3243}_{DFFB\ Saturated} \quad \underbrace{c_1 = 0.4944,\ c_2 = -0.4483}_{DFFB\ Superheated}$
Ganesan (neq) [11]	$h_{\text{tp}} = c_6 h_{DB_{g,a}}$ $h_{DB_{g,a}} = 0.023 \frac{k_{g,a}}{D} \text{Re}_{g,a}^{0.8} \text{Pr}_{g,a}^{0.4}, \quad \text{Re}_{g,a} = \frac{GDX_{v,a}}{\mu_{g,a}}, \quad \text{Pr}_{g,a} = \frac{\mu_{g,a} c_{p,g,a}}{k_{g,a}}$ $X_{v_a} = (c_1 + c_2 X_v + c_3 X_v^2 + c_4 X_v^3) \text{Fr}_{fo}^{c_5}, \quad \text{Fr}_{fo} = \frac{G^2}{\rho_f^2 g D}$ If $X_{v_a} > X_v$ then $X_{v_a} = X_v$, else if $X_{v_a} > 1$ then $X_{v_a} = 1$ Intersection $X_{v_a,int}$ between $X_{v_a} = X_v$ and $X_{v_a} = (c_1 + c_2 X_v + c_3 X_v^2 + c_4 X_v^3) \text{Fr}_{fo}^{c_5}$ If $X_{v_a} \leq X_{v_a,int}$ then $X_{v_a} = X_v$ $c_1 = -0.0179,\ c_2 = 1.0092,\ c_3 = -0.3130,\ c_4 = 0.0325,\ c_5 = 0.0640,\ c_6 = 0.8608$
Miropolskii [12]	$h_{\text{tp}} = 0.023 \text{Re}_{\text{mix}}^{0.8} \text{Pr}_g^{0.4} Y \frac{k_g}{D}$ $\text{Re}_{\text{mix}} = \left(\frac{GD}{\mu_g}\right) \left[X_v + \left(\frac{\rho_g}{\rho_f}\right)(1 - X_v)\right], \quad Y = 1 - 0.1 \left(\frac{\rho_f}{\rho_g} - 1\right)^{0.4} (1 - X_v)^{0.4}$
Groeneveld [13]	$h_{\text{tp}} = 0.00109 \text{Re}_{\text{mix}}^{0.989} \text{Pr}_g^{1.41} Y^{-1.15} \frac{k_g}{D}$ $\text{Re}_{\text{mix}} = \left(\frac{GD}{\mu_g}\right) \left[X_v + \left(\frac{\rho_g}{\rho_f}\right)(1 - X_v)\right], \quad Y = 1 - 0.1 \left(\frac{\rho_f}{\rho_g} - 1\right)^{0.4} (1 - X_v)^{0.4}$
Dougall-Rohsenow [8]	$h_{tp} = h_{\text{DB,g}} \Phi^{0.8}$ $h_{\text{DB,g}} = 0.023 \frac{k_g}{D} \text{Re}_g^{0.8} \text{Pr}_g^{0.4}, \quad \text{Re}_g = \frac{GD}{\mu_g}, \quad \text{Pr}_g = \frac{\mu_g c_{p,g}}{k_g}, \quad \Phi = X_v + (1 - X_v) \frac{\rho_g}{\rho_f}$
Hendricks [3]	$h_{\text{tp}} = \frac{h_{DB,fm}}{0.611 + 1.93 X_{tt,fm}}$ $h_{DB,fm} = 0.023 \frac{k_{g,fm}}{D} \text{Re}_{g,fm}^{0.8} \text{Pr}_{g,fm}^{0.4}, \quad \text{Re}_{g,fm} = \frac{GD}{\mu_{g,fm}}, \quad \text{Pr}_{g,fm} = \frac{\mu_{g,fm} c_{p,g,fm}}{k_{g,fm}}$ $\frac{1}{X_{tt,fm}} = \left(\frac{X_v}{1 - X_v}\right)^{0.9} \left(\frac{\rho_f}{\rho_{g,fm}}\right)^{0.5} \left(\frac{\mu_{g,fm}}{\mu_f}\right)^{0.1}, \quad T_{fm} = \frac{T_w + T_b}{2}$

7. Results

7.1. Smoothing

To obtain more realistic heat transfer coefficients around the CHF region, particularly in subcooled flows where film boiling correlations are used with a minimum vapour fraction, a smoothing function has been implemented.

Following the methodology outlined in [2], where a hyperbolic tangent function is used to smooth the heat transfer coefficient in the vicinity of the CHF, this study similarly employs a hyperbolic tangent approach. However, whereas [2] applies the smoothing to the thermal resistance (i.e., the inverse of the heat transfer coefficient), this study smooths the heat transfer coefficient itself. This modification aims to give more weight to the nucleate boiling coefficient, which typically has a much larger magnitude. In contrast, utilizing the thermal resistance would make the overall heat transfer coefficient less sensitive to the nucleate boiling coefficient, especially when the film boiling coefficient approaches zero. The equation used for the heat transfer coefficient is reported in Eq. 3.

$$h_c = h_{c,nb} - \frac{1}{2} \left[1 + \tanh\left(\frac{x - x_{CHF}}{k_{sm} D_h}\right)\right] (h_{c,nb} - h_{c,fb}) \tag{3}$$

The coefficient k_{sm} regulates the width of the region in the neighborhood of the CHF where the smoothing is applied. Through analyses conducted using experimental data from the reference works, it has been found that a correlation exists between the optimal k_{sm} that reduces the error with respect to the experimental data and the rate at which the vapor fraction increases. As a result, an investigation has been undertaken to establish a correlation with the Boiling number $Bo = q/(Gh_{fg})$.

The findings are presented in Fig. 5, showing the results of a linear fit. This fit takes the form detailed in Eq. 4, accompanied by its corresponding R^2 value.

$$k_{sm} = 781.2Bo + 1.552 \qquad R^2 = 0.79 \qquad (4)$$

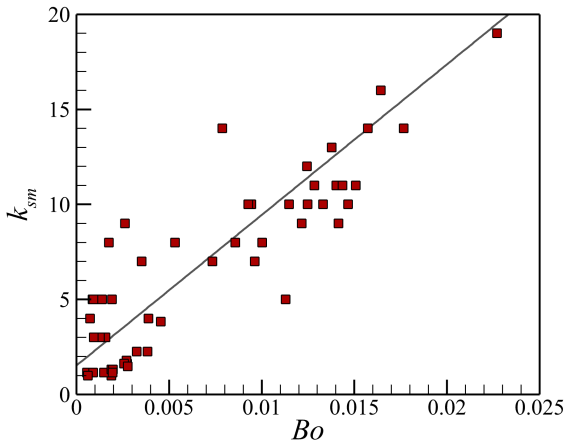

Figure 5: Linear fit for smoothing parameter k_{sm} as a function of Bo.

Eventually, to show the limitations of the correlations in case of CHF occurring at small bulk vapour fractions and to prove the efficacy of the present smoothing technique, in Fig. 6 are reported the wall temperature predictions with respect to reference data with and without smoothing for *Run 204* from [3] and *Run 210* from [5].

Results have been obtained with the correlation of *Ganesan (eq)* for the film boiling heat transfer coefficient. It is evident that significant discrepancies in wall temperature prediction arise especially in subcooled regions or areas characterized by low bulk vapour quality, leading to very large values of wall temperature. Conversely, employing the smoothing technique notably enhances predictions in the vicinity of the CHF condition, yielding substantial improvements.

7.2. Post-CHF heat transfer correlations

In this section, the new model is tested employing multiple correlations for film boiling heat transfer reported in Tab. 2. A comparison is also made with respect to the built-in `ht_tube` option.

Prior to delving into the examination of the CHF correlations utilized to determine the CHF location, it should be noted that the CHF position itself in the new component can be manually specified as an input by the user. Thus, focusing the study towards the predictive capabilities of the chosen correlations within their respective two-phase regimes of application, the current analysis has been conducted with the CHF position provided as input.

To assess the accuracy of the selected correlations, a comparison is made with respect to the reference data [3–5] by evaluating the Mean Absolute Error (MAE) as shown in Eq. 5.

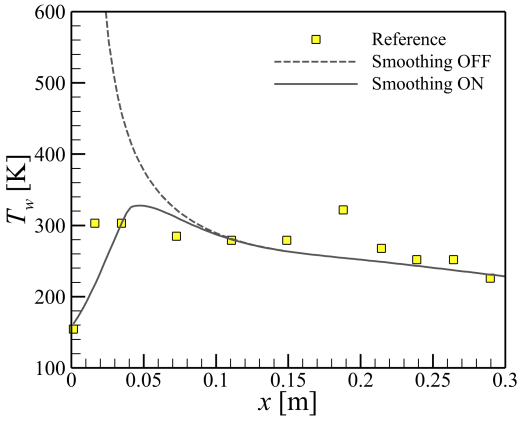

(a) Run 20-4 N_2 [3].

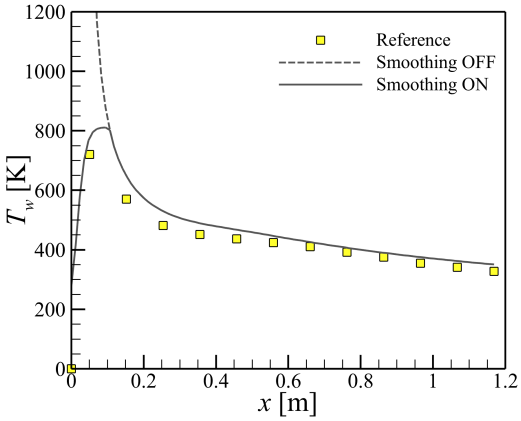

(b) Run 210 H_2 [5].

Figure 6: Smoothing technique.

$$\text{MAE} = \frac{1}{N_m} \sum_{i=1}^{N_m} \frac{|\phi_{p,i} - \phi_{m,i}|}{\phi_{m,i}} \times 100 \qquad (5)$$

where N_m is the number of measurements ϕ_p is the predicted value of the generic quantity ϕ and ϕ_m is the measured value of ϕ. The comparison has been carried out in terms of wall temperature ($\phi = T_w$) for each run.

Results of MAE are reported in Figs. 7-9, respectively for all the test cases of the reference works of [3], [4] and [5].

It can be noted that the worst result is the one obtained with built-in model, which adopts the Chen correlation for nucleate boiling until $X_v < 0.7$. As a matter of fact, the reference works are mainly devoted to the study of post-CHF scenarios. More precisely, CHF takes place essentially at the beginning of the pipe, where X_v is very small or even negative, meaning that CHF occurs when the fluid is still subcooled. Hence, the rationale behind the transition from nucleate boiling to film boiling regime adopted in the built-in model is clearly inappropriate for such

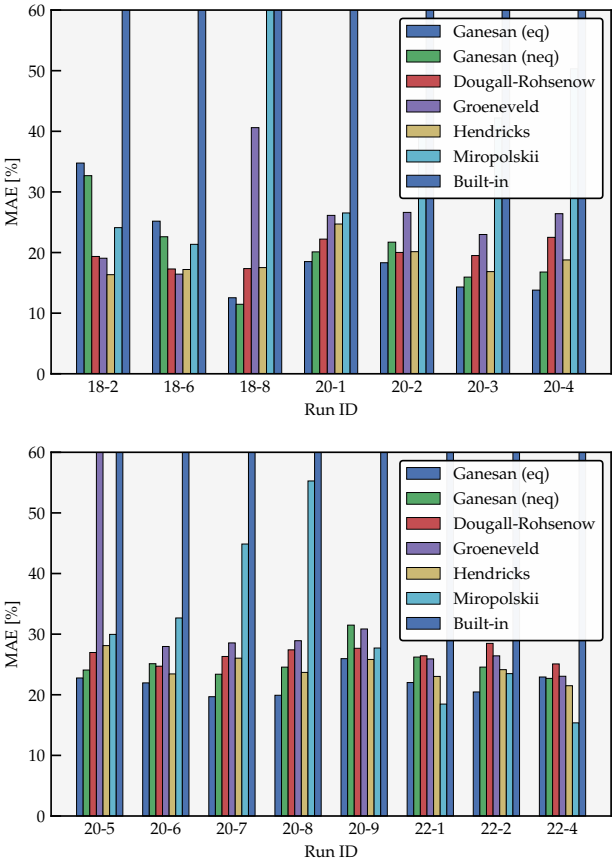

Figure 7: MAE calculated on test cases from [3].

class of applications. Comparing the different correlations it can be noted that all of them yield a great improvement in the prediction of heat transfer. Both correlations of Ganesan et al. [11], the correlation of Dougall-Rohsenow [8] and the correlation of Groeneveld [13] show good predictive capabilities for many test cases of both fluids, the correlation of Hendricks [3] performs well mainly with hydrogen data of [3] but on the contrary shows errors larger than 60% for all the test cases. Eventually the correlation of Miropolskii [12] shows good prediction only concerning few hydrogen cases.

To give a further insight about the predictive capabilities of the different correlations, the comparison between wall temperature prediction and reference data is reported in Figs. 10-12, respectively for all the test case of the reference works [3], [4] and [5].

The same conclusions drawn in the discussion of Figs. 7-9 can be observed here. Moreover it can be noted the large overprediction that is obtained with the built-in `ht_tube` model, that yields heat transfer coefficients between 1 and 2 orders of magnitude larger than the reference case. There are few points of the built-in model that are somehow in agreement with the reference data and those are the ones of test cases belonging to [4] and [5] where the bulk vapour fraction exceeds 0.7. Indeed, in such conditions the model selects the Dougall and Rohsenow correlation, which is suited for the film boiling regime.

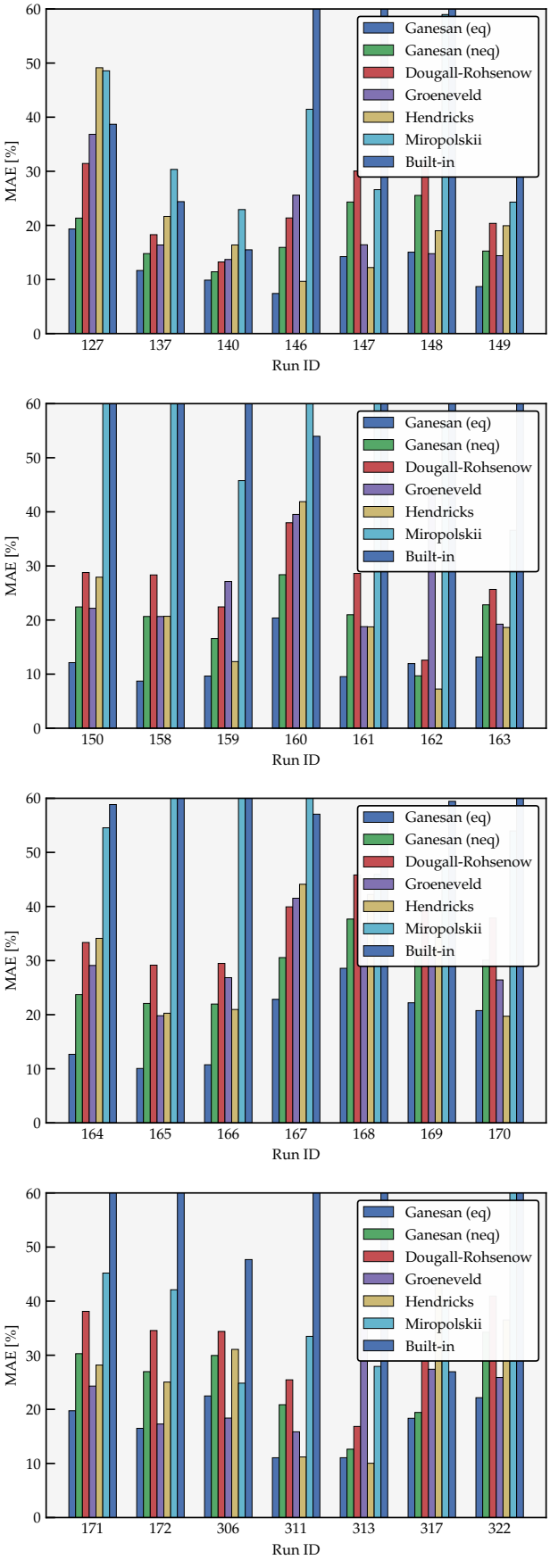

Figure 8: MAE calculated on test cases from [4].

Figs. 10-12 provide also valuable insights regarding the dispersion of predicted data points. It can

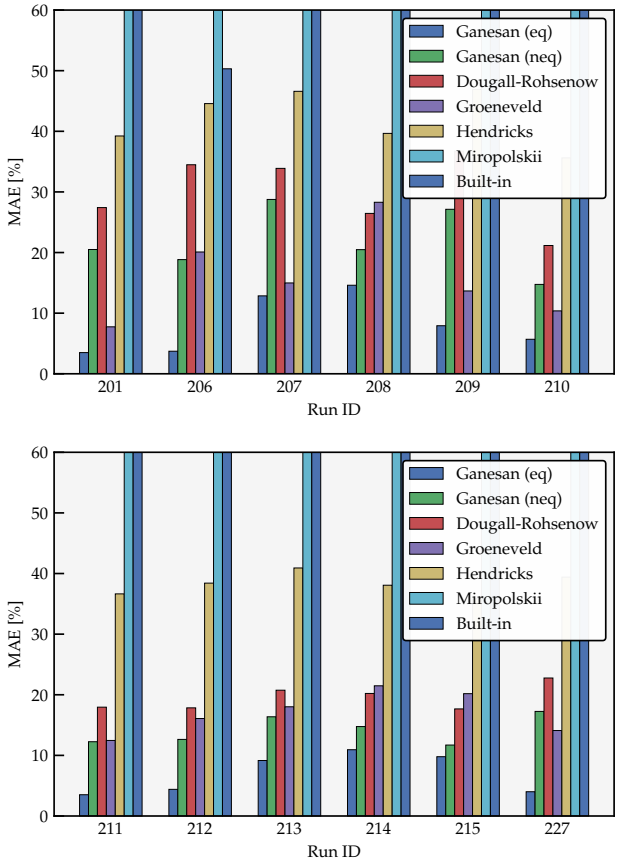

Figure 9: MAE calculated on test cases from [5].

be noted that the correlations of Ganesan et al. [11], especially the one based on the equilibrium assumption, *Ganesan (eq)*, globally show predictions which are rather concentrated around the reference data points. In contrast, the other correlations produce more dispersed results. In order to give a more precise quantification about how much predictions are spread for each test case the Root Mean Square Error (RMSE) is evaluated as reported in Eq. 6, using the same nomenclature adopted for the definition of MAE:

$$\text{RMSE} = \sqrt{\frac{1}{N_m}\sum_{i=1}^{N_m}\left(\frac{\phi_{p,i}-\phi_{m,i}}{\phi_{m,i}}\right)^2} \times 100 \qquad (6)$$

RMSE is shown for all test cases in Figs. 13-15.

Eventually, the overall MAE and RMSE are reported for each correlation in Tab. 3 and Tab. 4, respectively.

From the analysis performed it has been observed that the correlation which has shown to be more accurate in terms of MAE and RMSE is the *Ganesan (eq)*. Also the correlation *Ganesan (neq)* has shown overall good predictive capabilities but since has a more complex structure and thus it is more prone to numerical errors, the former correlation is preferred and eventually selected has a default option for film boiling heat transfer in the new developed component.

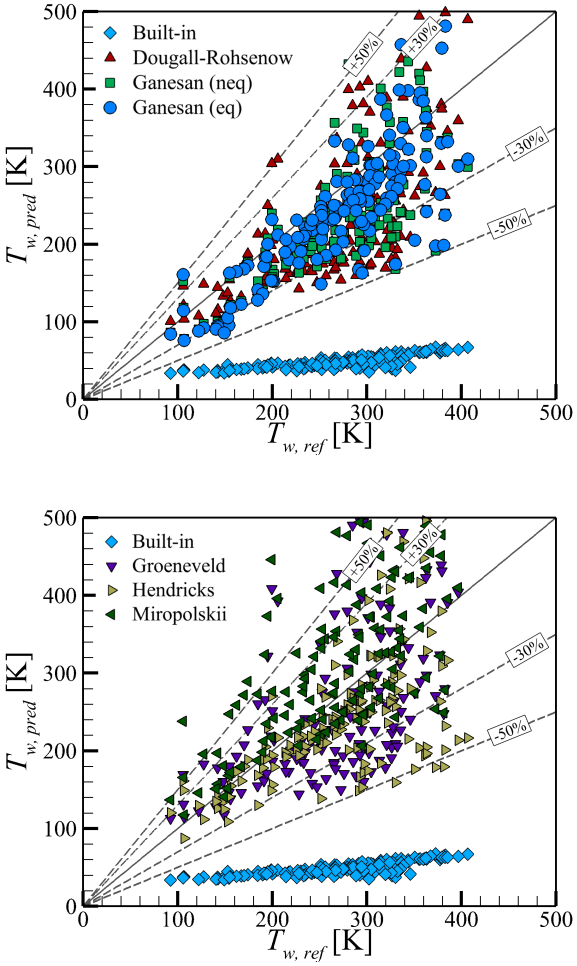

Figure 10: Test cases from [3].

Table 3: MAE calculated on the simulated run for each test case.

MAE [%]	H_2 [3]	H_2 [4]	N_2 [5]
Built-in	78.15	58.24	71.18
Ganesan (eq) [9]	20.79	15.03	7.51
Ganesan (neq) [9]	22.73	22.96	17.95
Dougall-Rohsenow [8]	23.19	29.49	24.78
Groeneveld [13]	33.59	25.10	16.46
Hendricks [3]	21.63	24.94	40.15
Miropolskii [12]	35.02	48.45	138.2

7.3. CHF position

In the previous section, predictive capabilities of multiple film boiling correlations have been assessed by fixing the experimental location of the CHF, in such a way a proper comparison is made against experimental data. However, CHF location is not usually known *a priori*, hence it has to be properly calculated by the present component. For this purpose, suitable correlations have to be selected. Specifically, the universal correlation of *Ganesan* [9] and the correlation of *Shah* [10] have been tested,

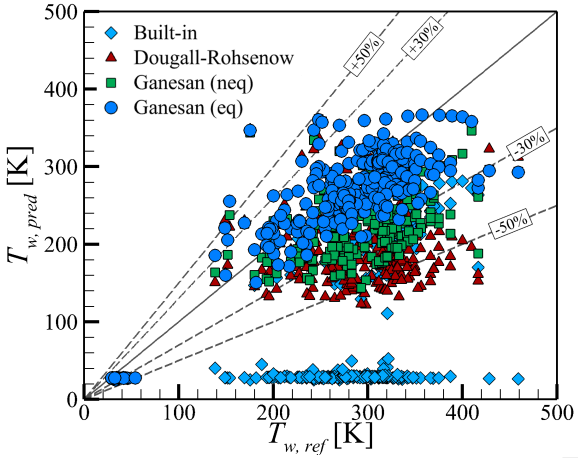

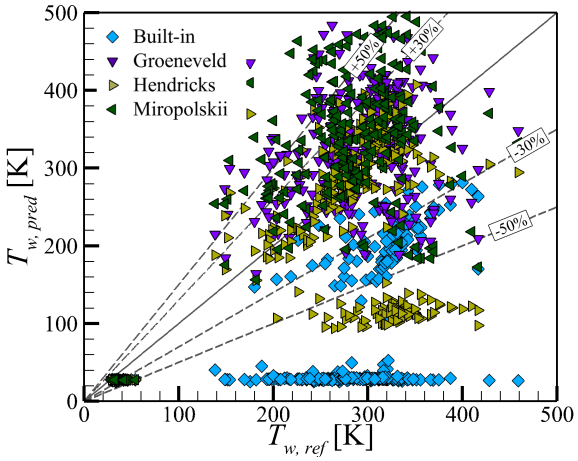

Figure 11: Test cases from [4].

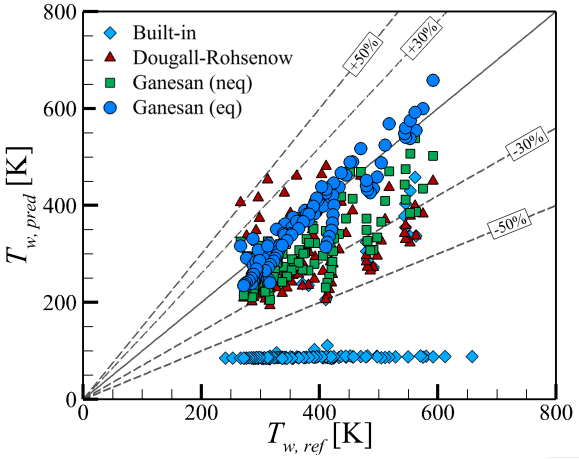

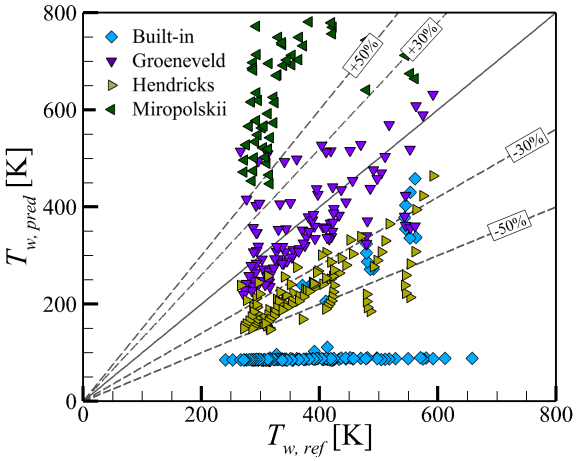

Figure 12: Test cases from [5].

Table 4: RMSE calculated on the all simulated runs for each test case.

RMSE [%]	H_2 [3]	H_2 [4]	N_2 [5]
Built-in	78.57	67.93	72.50
Ganesan (eq) [9]	28.97	30.10	9.42
Ganesan (neq) [9]	27.68	34.96	20.66
Dougall-Rohsenow [8]	26.84	42.41	27.75
Groeneveld [13]	47.70	41.65	21.68
Hendricks [3]	29.82	38.73	41.29
Miropolskii [12]	51.20	87.78	164.6

whose relations are reported in Tab. 1.

The error on the calculation of the CHF position is evaluated through Eq. 7 and results reported in Tab. 5 for each correlation and reference work.

$$\varepsilon_{CHF} = \min\left[100, \frac{|x_{CHF,m} - x_{CHF,p}|}{L} \times 100\right] \quad (7)$$

It can be noted that 100% error is obtained with the built-in model for the data of *Hendricks et al*. In this case, the vapor quality never exceeds 0.7, so CHF is never reached even if it actually occurs al-

Table 5: Error in the calculation of the CHF position.

ε_{CHF} [%]	H_2 [3]	H_2 [4]	N_2 [5]
Built-in	100	50.2	94.8
Ganesan [9]	18.85	23.1	35.6
Shah [10]	0	22.4	81.6

ways at the inlet section of the channel. A bad performance is also observed concerning the nitrogen test cases, while a better agreement is obtained for hydrogen test cases of *Lewis et al*. The correlation of *Ganesan* shows rather good predictive capabilities, with an average accuracy of about 20% with respect to hydrogen reference works. A larger error is observed for the nitrogen test cases, which exhibit CHF always at the inlet section of channel. The correlation of *Shah* correctly predicts all the test cases of *Hendricks et al*, since for all the test cases the calculated critical heat flux is lower than the enforced value. A good performance is observed for the hydrogen cases of *Lewis et al*, while it exhibits a large error in the prediction of the nitrogen cases.

Eventually, Tab. 6 presents the Mean Absolute Error (MAE) calculated on wall temperature, com-

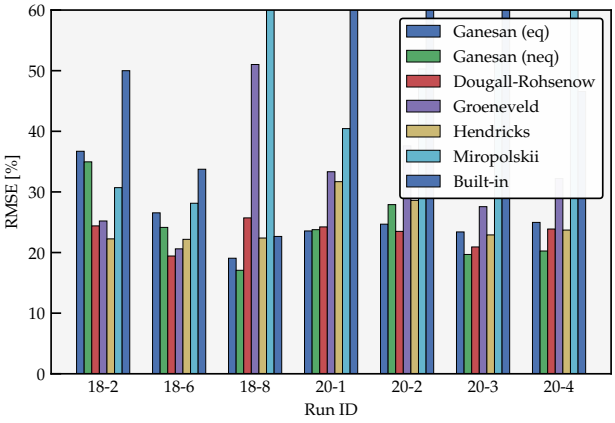

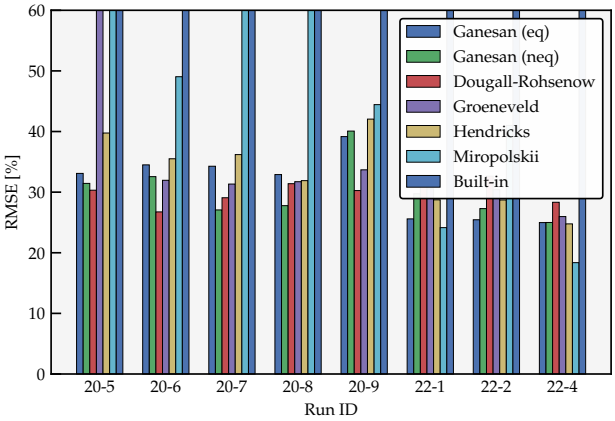

Figure 13: RMSE calculated on test cases from [3].

paring the Built-in model with the new model. The correlations used for the new model are those which have demonstrated the best overall accuracy across all test cases, encompassing both CHF position and post-CHF heat transfer. These correlations are the universal ones proposed by *Ganesan et al* [9, 11].

Table 6: Comparison of MAE calculated with the built-in model and the new model.

MAE [%]	H_2 [3]	H_2 [4]	N_2 [5]
Built-in	78.15	58.24	71.18
New model	35.38	42.43	22.65

It is evident that the error in the CHF position clearly deteriorates the accuracy reported in Tab. 3 concerning the *Ganesan (eq)* correlation. However, a substantial enhancement is obtained compared to the built-in model, particularly in the hydrogen test cases of *Hendricks* and the nitrogen test cases. Although there is an improvement also observed for the *Lewis* test cases, it seems to be less pronounced. It is important to stress out again that the built-in model determines the CHF position solely based on the bulk vapor fraction, which is not a suitable discriminant for the CHF phenomenon.

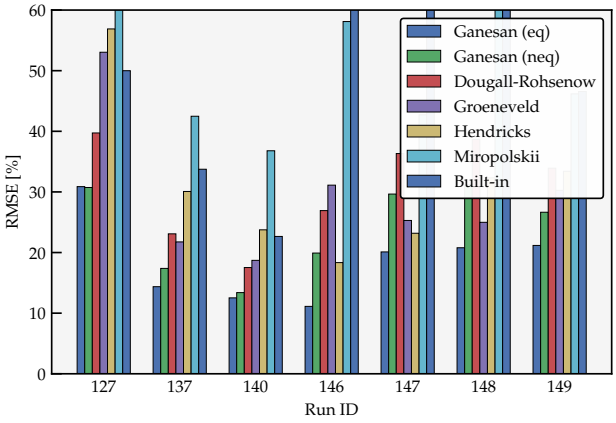

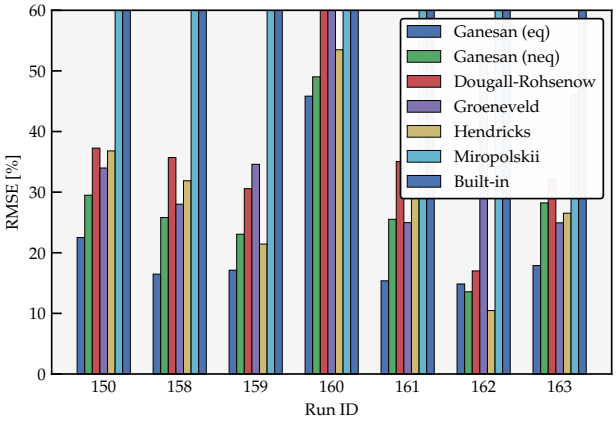

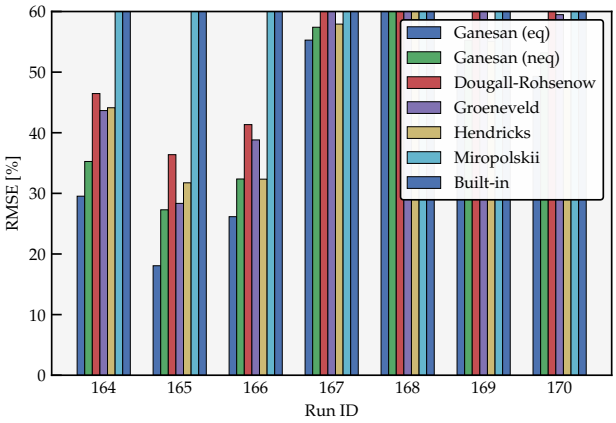

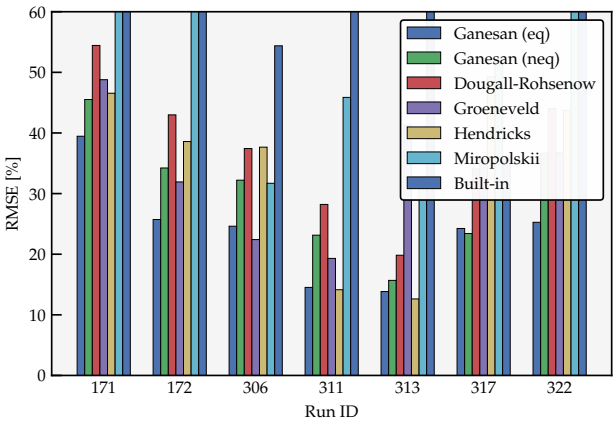

Figure 14: RMSE calculated on test cases from [4].

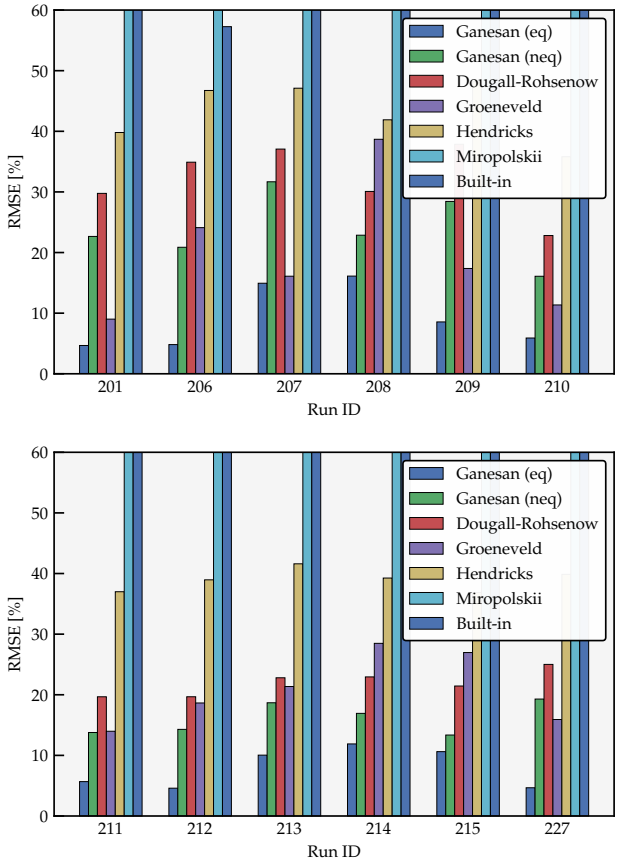

Figure 15: RMSE calculated on test cases from [5].

8. Conclusions

The present work introduces a new model, implemented within the EcosimPro/ESPSS framework, for analyzing two-phase heat transfer during flow boiling in cooling channels, with special attention to CHF and post-CHF regimes. Large limitations of the built-in heat transfer model have been observed in the prediction of post-CHF boiling flows. Hence, an improved model has been developed following a rationale where CHF is calculated rather that arbitrarily set to a fixed bulk vapour quality. Different correlations for film boiling heat transfer have been compared in terms of a MAE and RMSE, showing how heat transfer prediction can be greatly improved with respect to the original model. However, it must be pointed out that some steps are still needed to get a full characterization of the present model, testing the developed model on more realistic cases in the framework of flow boiling in liquid rocket propulsion components. Moreover, an extension to study two-phase transient operations is still missing. Particular attention must be devoted to the selection of suitable correlations. This further step will allow to extend the validity of the present component to interesting applications like chill-down operations. Eventually, an additional step involves a comprehensive evaluation of two-phase pressure drop models to enhance the predictive accuracy of the current model, aiming for less conservative designs.

References

[1] *ESPSS EcosimPro Libraries User Manual 3.4.0*. Comp. software. 2020.

[2] E. M. Tesny et al. “Validation of Universal Cryogenic Flow Boiling Correlations in Thermal Desktop for Liquid Hydrogen”. In: *AIAA SCITECH 2024 Forum*. 2024.

[3] R. Hendricks et al. “Experimental heat transfer and pressure drop of film boiling liquid hydrogen flowing through a heated tube”. In: *NASA Technical Note D-765*. 1961.

[4] J. P. Lewis, J. H. Goodykoontz, and J. F. Kline. *Boiling heat transfer to liquid hydrogen and nitrogen in forced flow*. National Aeronautics and Space Administration, 1962.

[5] R. P. Forslund and W. M. Rohsenow. “Thermal non-equilibrium in dispersed flow film boiling in a vertical tube”. In: *Technical Report 75312-44, Department of Mechanical Engineering Massachusetts Institute of Technology*. 1966.

[6] J. G. Collier and J. R. Thome. *Convective boiling and condensation*. Clarendon Press, 1994.

[7] J. C. Chen. “Correlation for boiling heat transfer to saturated fluids in convective flow”. In: *Industrial & engineering chemistry process design and development* 5.3 (1966), pp. 322–329.

[8] R. Dougall and W. Rohsenow. *Film boiling on the inside of vertical tubes with upward flow of the fluid a low qualities*. Tech. rep. Massachussetts Institute of Technology, 1963.

[9] V. Ganesan et al. “Universal critical heat flux (CHF) correlations for cryogenic flow boiling in uniformly heated tubes”. In: *International Journal of Heat and Mass Transfer* 166 (2021).

[10] M. M. Shah. “Improved general correlation for critical heat flux during upflow in uniformly heated vertical tubes”. In: *International Journal of Heat and Fluid Flow* 8.4 (1987), pp. 326–335.

[11] V. Ganesan et al. “Universal Correlations for Post-CHF Saturated and Superheated Flow Film Boiling Heat Transfer Coefficient, Minimum Heat Flux and Rewet Temperature for Cryogenic Fluids in Uniformly Heated Tubes”. In: *International Journal of Heat and Mass Transfer* 195 (2022).

[12] Z. Miropolskii. “Heat transfer in film boiling of a steam–water mixture in steam generating tubes”. In: *Teploenergetika* 10 (1963).

[13] C. W. Snoek and D. C. Groeneveld. “A comprehensive examination of heat transfer correlations suitable for reactor safety analysis”. In: *Multiphase Science and Technology* 2.1-4 (1986), pp. 181–274.

Appendix

Table A1: Operating conditions of reference test cases. H_2 [3, 4] and N_2 [5].

Run ID	Fluid	p_{out} [bar]	T_{in} [K]	G [kg/(sm^2)]	q [kW/m^2]	x_{CHF} [m]
18-2	H_2 [3]	2.6	25.0	1617.4	384.3	0.0
18-6	H_2 [3]	2.8	25.0	1653.9	630.6	0.0
18-8	H_2 [3]	1.9	24.0	804.1	641.1	0.0
20-1	H_2 [3]	2.9	24.0	1553.3	977.1	0.0
20-2	H_2 [3]	2.6	24.0	1242.7	986.8	0.0
20-3	H_2 [3]	1.9	24.5	858.9	990.9	0.0
20-4	H_2 [3]	1.6	24.0	721.9	994.3	0.0
20-5	H_2 [3]	3.3	23.5	1626.5	1354.0	0.0
20-6	H_2 [3]	2.6	24.0	1206.1	1376.2	0.0
20-7	H_2 [3]	1.9	24.5	849.8	1376.2	0.0
20-8	H_2 [3]	1.6	24.5	712.7	1370.7	0.0
20-9	H_2 [3]	3.2	24.0	1516.8	1650.6	0.0
22-1	H_2 [3]	3.4	25.0	1297.5	1514.8	0.0
22-2	H_2 [3]	2.6	25.5	922.9	1517.6	0.0
22-4	H_2 [3]	3.2	25.5	1379.7	1140.6	0.0
127	H_2 [4]	2.07	22.0	4.028	38.6	0.0423
137	H_2 [4]	3.45	24.6	5.479	32.5	0.1692
140	H_2 [4]	3.44	24.6	5.561	29.3	0.2227
146	H_2 [4]	3.52	24.1	14.78	59.0	0.0
147	H_2 [4]	5.03	25.9	17.36	70.7	0.0
148	H_2 [4]	5.03	25.8	13.14	67.5	0.0
149	H_2 [4]	4.89	26.5	14.58	79.2	0.0
150	H_2 [4]	4.89	26.9	14.58	76.7	0.0
158	H_2 [4]	3.52	23.6	10.97	66.6	0.0
159	H_2 [4]	3.58	23.8	17.77	69.7	0.0
160	H_2 [4]	3.72	24.1	7.093	49.8	0.0
161	H_2 [4]	3.52	21.8	8.707	55.5	0.0
162	H_2 [4]	2.07	21.7	18.31	60.9	0.0
163	H_2 [4]	2.14	21.7	18.31	77.6	0.0
164	H_2 [4]	3.58	23.7	8.219	57.1	0.0
165	H_2 [4]	3.58	23.8	11.77	66.2	0.0
166	H_2 [4]	3.45	21.7	11.38	66.2	0.0
167	H_2 [4]	3.58	21.7	7.825	57.1	0.0
168	H_2 [4]	4.89	21.7	10.01	74.8	0.0
169	H_2 [4]	4.89	21.7	11.05	73.5	0.0
170	H_2 [4]	4.76	24.5	20.61	74.7	0.0
171	H_2 [4]	4.48	25.2	9.521	59.0	0.0
172	H_2 [4]	4.83	25.3	11.45	68.5	0.0
306	H_2 [4]	3.31	23.9	10.84	51.7	0.1915
311	H_2 [4]	3.56	23.5	18.15	56.3	0.1057
313	H_2 [4]	3.51	22.9	21.97	49.4	0.0705
317	H_2 [4]	3.59	24.2	5.181	40.8	0.1226
322	H_2 [4]	3.55	25.3	11.80	57.3	0.0352
201	N_2 [5]	1.63	79.4	173.5	63.9	0.0
206	N_2 [5]	1.63	80.6	92.7	62.9	0.0
207	N_2 [5]	1.68	81.7	94.5	32.0	0.0
208	N_2 [5]	1.67	80.2	96.5	16.1	0.0
209	N_2 [5]	1.66	80.0	94.8	47.9	0.0
210	N_2 [5]	1.56	78.9	257.8	78.0	0.0
211	N_2 [5]	1.60	78.9	259.0	62.9	0.0
212	N_2 [5]	1.62	79.4	260.4	46.9	0.0
213	N_2 [5]	1.69	80.6	176.7	31.4	0.0
214	N_2 [5]	1.71	80.6	170.3	24.1	0.0
215	N_2 [5]	1.65	80.0	260.1	31.2	0.0
227	N_2 [5]	1.65	78.9	178.3	47.9	0.0